

Hydrodynamic afterburner for the Color Glass Condensate and the parton energy loss

Tetsufumi Hirano¹ and Yasushi Nara²

¹*RIKEN BNL Research Center, Brookhaven National Laboratory, Upton, New York 11973, USA*

²*Department of Physics, University of Arizona, Tucson, Arizona 85721, USA*

(Dated: September 5, 2018)

We take hydrodynamic initial conditions in relativistic heavy ion collisions from the Color Glass Condensate (CGC) picture through the k_T factorization formula. Gluon distributions produced from the CGC are found to provide good initial conditions for the hydrodynamic simulations in Au + Au collisions at Relativistic Heavy Ion Collider (RHIC) energies. We reproduce the centrality, rapidity, and energy dependences of multiplicity within this approach. We also investigate the energy loss of high p_T partons in the dense thermalized medium created from colliding two CGC's. We find that our results on the centrality dependence of nuclear modification factors for pions and back-to-back correlation for charged hadrons at midrapidity are consistent with the RHIC data up to semicentral events. Whereas, our approach in which jets are calculated from perturbative QCD $2 \rightarrow 2$ processes predicts less suppression at forward rapidity region compared to the BRAHMS data in Au+Au collisions at RHIC.

PACS numbers:

I. INTRODUCTION

Experiments of high energy pp , dA , and AA collisions are currently performed at the Relativistic Heavy Ion Collider (RHIC) in Brookhaven National Laboratory for comprehensive understanding of the highly hot/dense matter, the quark gluon plasma (QGP). At collider energies, collisions of two relativistic nuclei involve many aspects of physics according to the relevant energy or time scale. There already exist many theoretical approaches to understand numerous RHIC data. We consider in this work, particularly, the physics of the gluon saturation in a colliding nucleus, hydrodynamic evolution of produced matter, and the energy loss of hard partons in the medium. Our goals are to combine them and to take a first step toward a unified understanding of the dynamical aspect of high energy heavy ion collisions.

First data reported by the STAR Collaboration at RHIC [1] revealed that the observed large magnitude of elliptic flow for hadrons is naturally explained by hydrodynamics. This suggests that large pressure possibly in the partonic phase is built at the very early stage ($\tau \sim 0.6$ fm/ c) in Au+Au collisions at RHIC. This is one of the strongest indications of early thermalization of the QGP at RHIC [2, 3]. These hydrodynamic predictions also give good agreements with mass dependences of the second harmonic coefficient of azimuthal distribution $v_2(p_T)$ in the low p_T region [4]. This is in contrast to the case in the lower energy collisions where the hydrodynamics always overpredicts the data [5, 6]. Hydrodynamics also predicts that the scaled elliptic flow, which is defined as the second harmonics v_2 divided by initial spatial eccentricity ε , becomes almost constant around 0.2 [7]. The experimental data reaches the hydrodynamic limit for the first time in central and semicentral collisions at RHIC energies [8]. Moreover, v_2 as a function of pseudorapidity [9] can be reproduced by hydrodynamics only in $|\eta| < 1$ [10]. All these analyses indicate that a high dense matter created

in heavy ion collisions at RHIC energies achieves (local) thermal equilibrium state in the low p_T region, around midrapidity, and up to semicentral collisions.

On the other hand, jet production rate becomes large enough to measure high p_T power-law tails at RHIC. These minijets go across the expanding matter rather than participate in the dense medium in the case of heavy ion collisions. During traveling through the expanding medium, energetic partons interact with soft matter and lose their energies dynamically (jet quenching). Thus, high p_T hadrons coming from fragmentation of minijets can be good probes of the bulk matter [11]. It was observed that nuclear modification factors for hadrons in the high $p_T > 5$ GeV/ c region are considerably smaller than unity in central collisions [12, 13, 14, 15] and that it increases with decreasing centrality and eventually reaches around unity in peripheral collisions. Disappearance of the away-side peak in azimuthal correlation functions for high p_T hadrons is also observed in central Au+Au collisions [16]. This can be described by perturbative QCD (pQCD) based parton models with parton energy loss in the dense medium [17, 18, 19]. Cronin enhancement of the hadron spectra and existence of the back-to-back correlation at mid-rapidity in dA collisions at RHIC [15, 20, 21, 22] support that suppression of the yield and disappearance of the away-side peak in Au+Au collisions at mid-rapidity are due to the final state interaction. The radiative parton energy loss induced by the medium has been studied extensively [23, 24, 25, 26, 27, 28] and found that the energy loss is proportional to the gluon rapidity density of the medium. Theoretical analyses reveal that a large parton energy is required to account for observed suppressions of single as well as dihadron spectra at RHIC [19, 29, 30].

From the above discussion, the current RHIC data strongly suggest that the parton density created in heavy ion collisions at RHIC is dense enough to cause both large elliptic flow of bulk matter and large suppression of

high- p_T hadrons. One of the important problems in the physics of heavy ion collisions is to reveal the origin of this dense matter. The bulk particle production in high energy hadronic collisions is dominated by the small x modes in the nuclear wave function, where x is a momentum fraction of the incident particles. Therefore, an origin of the large density could be traced to the initial parton density at small x inside the ultra-relativistic nuclei before collisions [31]. It is well known that gluon density increases rapidly with decreasing x by the BFKL cascade until gluons begin to overlap in phase space [32] where nonlinear interaction becomes important. These gluons eventually form the Color Glass Condensate (CGC) [33]. This phenomenon is characterized by a ‘‘saturation scale’’ Q_s^2 which corresponds to the gluon rapidity density per unit transverse area. When Q_s^2 is large ($Q_s \gg \Lambda_{\text{QCD}}$), the coupling becomes weak ($\alpha_s(Q_s) \ll 1$). In addition, the gluon occupation number in the wave function is huge, $\sim 1/\alpha_s(Q_s) \gg 1$. Therefore this can be studied by an weak coupling classical method known as McLerran-Venugopalan (MV) model [34]. It has been developed to compute the classical parton distributions of nuclei based on this model. Moreover, renormalization group methods which systematically incorporate quantum corrections to the classical effective theory were developed [35, 36, 37]. There is an evidence for gluon saturation in deep inelastic scattering at HERA. Models based on the saturation picture fit the HERA data well in the moderate Q^2 and low x [38, 39]. This effective theory can be applied to the collisions of nuclei and its solution can be used for initial conditions of further evolution of the system created in heavy ion collisions [40, 41, 42, 43]. Perturbative solutions of the gluon production for collisions of two nuclei [44, 45] as well as pA collisions [46, 47] have been computed. Non-perturbative classical solutions of the Yang-Mills equations were also obtained by the real-time numerical simulations on the lattice [48, 49, 50]. The calculations based on the CGC picture have been compared to various RHIC data. Remarkably, the CGC results on the global observables, e.g., the centrality, rapidity and energy dependences of charged hadron multiplicities agree with the RHIC data under the assumption of parton-hadron duality [51]. The CGC picture is also applied for studies of particle correlations and azimuthal anisotropies [52], and valence quark distributions at small- x [53]. It has been shown that the classical wave function in the MV model contains Cronin enhancement and that quantum evolution with respect to x makes the spectrum suppressed [54, 76]. Suppression of nuclear modification factor at forward rapidity region in dA collisions [55] in the CGC picture is also consistent with the recent RHIC data [56].

The above facts show that the CGC, hydrodynamics, and the energy loss of hard partons are the key ingredients to describe the RHIC physics. One expects that they are indeed closely related with each other. For example, the CGC could be a good initial condition for a thermalized state because it produces a large number of

gluons. Thus a large number of gluons are responsible for large suppression of jet spectra. In order to understand systematically the whole of the stages of relativistic heavy ion collisions, it is indispensable to construct a unified and dynamical framework in which the above different ideas are consistently incorporated. In this work, we perform hydrodynamic simulations with the initial condition taken from the CGC and simulate parton energy loss in the fluid elements. This approach will lead us to get deeper understanding of the dynamical aspect of heavy ion collisions.

In addition, some of the problems which are inherent in a particular approach can be removed. For instance, one conventionally parametrizes initial conditions in the hydrodynamic simulations shortly after a collision of two nuclei so as to reproduce final observed spectra. Hydrodynamic framework itself does not provide an initial condition. Hence one has to choose it from infinite possible candidates. Any initial conditions which reproduce the final hadron spectra are equivalent, so it is hard to discard even one of them within the hydrodynamic approach. This is the ambiguity problem of hydrodynamic model in heavy ion collisions. A good example can be found in Ref. [57]: Two completely different initial conditions end up almost the same rapidity distribution. Therefore it is desired to take an initial condition which is obtained by a reliable theory. On the other hand, most of the calculations based on the CGC do not include final state interactions. According to estimation of initial parton productions from a classical lattice Yang-Mills simulation based on the CGC [50, 58], the transverse energy per particle is roughly $E_T/N \sim 1.5$ GeV, while the experimental data yields $E_T/N \sim 0.6$ GeV [60]. The elliptic flow from a classical Yang-Mills simulation is inconsistent with RHIC data [59]. Those discrepancies, which are mainly due to the lack of collective effects, will be removed by introducing further time evolutions through, e.g., hydrodynamics.

For the calculation of parton energy loss, one needs time evolution of parton density. Bjorken expansion [61] is assumed for the evolution of parton density in almost all work except Ref. [62] in which hydrodynamic simulations are used to estimate the energy loss of partons for the first time. We have previously established a model (the hydro+jet model) in which hydrodynamic evolutions are combined with explicitly traversing non-thermalized partons with large transverse momenta [17, 63, 64, 65]. Here the production of high p_T partons is described by a pQCD parton model. These high p_T partons come from parton distribution function in relatively large x region. Systematic studies based on the hydro+jet model have been performed for p_T spectra [65], back-to-back correlation functions [17], pseudorapidity dependence of nuclear modification factors [64], and elliptic flow [64, 65]. For the initial condition of hydrodynamic simulations, we simply parametrized the initial shape of energy density in the previous work. Instead, we will employ the CGC picture and use gluons produced from melting CGC for

initial conditions for hydrodynamic simulations in this paper. The number and the energy density distributions for produced gluons are calculated from the k_T factorization formula [51]. Although the produced gluons will reach a thermalized state through the dissipative processes in the realistic situations, the description of non-equilibrium phenomena is beyond the scope of the present paper. Instead, we assume thermalization for gluons produced from the CGC.

This paper is organized as follows. In Sec. II, we discuss how the gluon distribution produced from the CGC is used for the initial condition in the hydrodynamics. In Sec. III, we briefly summarize the hydro+jet model. In Sec. IV, we present hydrodynamic results on (pseudo)rapidity distributions for charged hadrons and the transverse momentum distributions for pions, kaons, and protons. We show that the CGC provides good initial conditions in the hydrodynamic model. We also show that, with almost keeping the shape of rapidity distribution during the hydrodynamical evolution, transverse collective flow is generated by pressure gradient perpendicular to the collision axis. We study the centrality dependence of the nuclear modification factor for neutral pions and the back-to-back correlations for charged hadrons. The previous analysis on the high p_T hadron spectra in the forward rapidity region is revisited. In the final section, we give a summary and a discussion about the further improvements in our approach.

II. INITIAL CONDITION FOR HYDRODYNAMICS FROM GLUON SATURATION

There exists a lot of extensive work for the description of gluon productions in nuclear collisions in the saturation regime where nonlinear effects become important. Perturbative solutions for the collision of two nuclei in the MV model were obtained in Refs. [44, 45]. However, those solutions are limited for the relatively high momentum and cannot be used for the calculation of total gluon multiplicities. In Ref. [66], analytic expression for the gluon multiplicity is obtained. Non-perturbative classical boost invariant solutions are currently available on the lattice [48, 49, 50, 58] and it is highly desired to use the lattice results for obtaining reliable initial conditions. However, one of our purposes in this paper is to investigate the rapidity dependence of final hadrons. Therefore, we employ the k_T factorization formula along the line of work done by Kharzeev, Levin, and Nardi (KLN) [51] for the computation of the gluon rapidity distribution which is to be the initial condition for sequential hydrodynamic evolution.

A. Gluon Production in the k_T factorization formula

The number of produced gluons in the k_T -factorization formula is given by [32, 67, 68, 69]

$$\begin{aligned} \frac{dN_g}{d^2x_\perp dy} &= \frac{4\pi^2 N_c}{N_c^2 - 1} \int \frac{d^2 p_T}{p_T^2} \int d^2 k_T \alpha_s(Q^2) \\ &\times \phi_A(x_1, k_T^2; \mathbf{x}_\perp) \phi_B(x_2, (p_T - k_T)^2; \mathbf{x}_\perp), \end{aligned} \quad (1)$$

where $x_{1,2} = p_T \exp(\pm y)/\sqrt{s}$ and y and p_T are a rapidity and a transverse momentum of a produced gluon. Running coupling α_s is evaluated at the scale $Q^2 = \max(k_T^2, (p_T - k_T)^2)$. The unintegrated gluon distribution ϕ is related to the gluon density of a nucleus by

$$xG_A(x, Q^2) = \int^{Q^2} d^2 k_T d^2 x_\perp \phi_A(x, k_T^2; \mathbf{x}_\perp). \quad (2)$$

There are several models/parametrizations in the literature which provide a gluon distribution in the saturation region. In principle, the x dependence of unintegrated distribution functions in Eq. (1) should be solutions to the nonlinear quantum evolution equations such as Balitsky-Kovchegov equation [70, 71] or, more generally, JIMWLK equation [35, 36, 37]. Leaving this analysis for the future work, we follow basically the KLN approach which captures the essential features of the gluon saturation physics in a simple manner.

In the MV model [34], the gluon distribution below the saturation scale Q_s^2 is logarithmically suppressed $\phi(k_T^2) \sim \ln(Q_s^2/k_T^2)$ compared to the perturbative distribution $\sim 1/k_T^2$. Instead, motivated by the KLN approach, we use a simplified assumption about the unintegrated gluon distribution function:

$$\phi_A(x, k_T^2; \mathbf{x}_\perp) = \begin{cases} \frac{\kappa C_F}{2\pi^3 \alpha_s(Q_s^2)} \frac{Q_s^2}{Q_s^2 + \Lambda^2}, & k_T \leq Q_s, \\ \frac{\kappa C_F}{2\pi^3 \alpha_s(Q_s^2)} \frac{Q_s^2}{k_T^2 + \Lambda^2}, & k_T > Q_s, \end{cases} \quad (3)$$

where $C_F = (N_c^2 - 1)/(2N_c)$. We introduce a small regulator $\Lambda = 0.2 \text{ GeV}/c$ in order to have a smooth distribution in the forward rapidity region $|y| > 4.5$ at RHIC. Other regions are not affected by introducing a small regulator. As we will discuss below, the above distribution depends on the transverse coordinate \mathbf{x}_\perp through Q_s^2 . We are interested in the centrality and rapidity dependences of total yields which are dominated by the low transverse momenta. The above simple form should be fine for this purpose, although the effect of anomalous dimension resulting from the presence of the CGC modifies the p_T dependence of the produced gluons as shown in Ref. [72, 73, 74, 75, 76]. An overall constant factor κ is determined by fitting the multiplicity of charged hadron at midrapidity at $\sqrt{s_{NN}} = 200 \text{ GeV}$ for the most central collision. Saturation momentum of a nucleus A in

$A + B$ collisions is obtained by solving the following implicit equation with respect to Q_s at fixed x and \mathbf{x}_\perp

$$Q_s^2(x, \mathbf{x}_\perp) = \frac{2\pi^2}{C_F} \alpha_s(Q_s^2) x G(x, Q_s^2) \rho_{\text{part}}^A(\mathbf{x}_\perp), \quad (4)$$

where

$$\rho_{\text{part}}^A(\mathbf{x}_\perp) = T_A(\mathbf{x}_\perp) \{1 - [1 - \sigma_{NN}^{\text{in}} T_B(\mathbf{x}_\perp)/B]^B\}. \quad (5)$$

The number of participants is given by

$$N_{\text{part}} = \int d^2x_\perp (\rho_{\text{part}}^A(\mathbf{x}_\perp) + \rho_{\text{part}}^B(\mathbf{x}_\perp)). \quad (6)$$

We take a simple perturbative form for the gluon distribution for a nucleon

$$xG(x, Q^2) = K \ln \left(\frac{Q^2 + \Lambda^2}{\Lambda_{\text{QCD}}^2} \right) x^{-\lambda} (1-x)^n \quad (7)$$

where $\Lambda = \Lambda_{\text{QCD}} = 0.2$ GeV. K is used to control saturation scale in Eq. (4) [76]. We choose $K = 0.7$ for $\lambda = 0.2$ ($K = 0.55$ for $\lambda = 0.25$ or $K = 0.44$ for $\lambda = 0.3$) so that average saturation momentum in the transverse plane yields $\langle Q_s^2(x = 0.01) \rangle \sim 2.0$ GeV²/c² in Au+Au collisions at impact parameter $b = 0$ at RHIC. Similar to the KLN approach, $x^{-\lambda}$ dependence of the saturation scale is motivated by the Golec-Biernat–Wüsthoff model [38]. The factor $(1-x)^n$ shows that gluon density becomes small at $x \rightarrow 1$. n usually depends on the scale Q^2 . Here we take $n = 4$ as in the KLN approach [51].

We obtain the rapidity distribution for produced gluons at each transverse point \mathbf{x}_\perp by performing the integral of Eq. (1) numerically. The transverse energy distribution dE_T/dy is also obtained by weighting the transverse momentum of gluons p_T in the integration with respect to p_T in Eq. (1). We cut off the integral range of p_T in Eq. (1) since only the low p_T partons are assumed to reach the local thermal equilibrium. Instead, hard partons are included by assuming usual pQCD $2 \rightarrow 2$ processes in which DGLAP evolution is included as it is important in the high Q^2 reactions. It is unclear which value we have to use for the cut off momentum $p_{T,\text{cut}}$, because it contains a nonperturbative nature and also it would depend on the choice of unintegrated wave function. We set the cut off momentum at $p_{T,\text{cut}} = 3$ GeV/c which corresponds roughly to the maximum saturation scale at $x = 0.01$ at the origin $\mathbf{x}_\perp = \mathbf{0}$ in central Au+Au collisions at RHIC.

Figure 1 (a) shows rapidity distributions of produced gluons obtained from Eq. (1). Assuming free streaming in the longitudinal direction until $\tau = 0.6$ fm/c, we also obtain the number density and the energy density as functions of a transverse coordinate as shown in Fig. 1 (b). Here the direction of the x -axis is the same as that of the impact parameter vector. Solid (dashed) line corresponds to the number (energy) distribution of produced gluons.

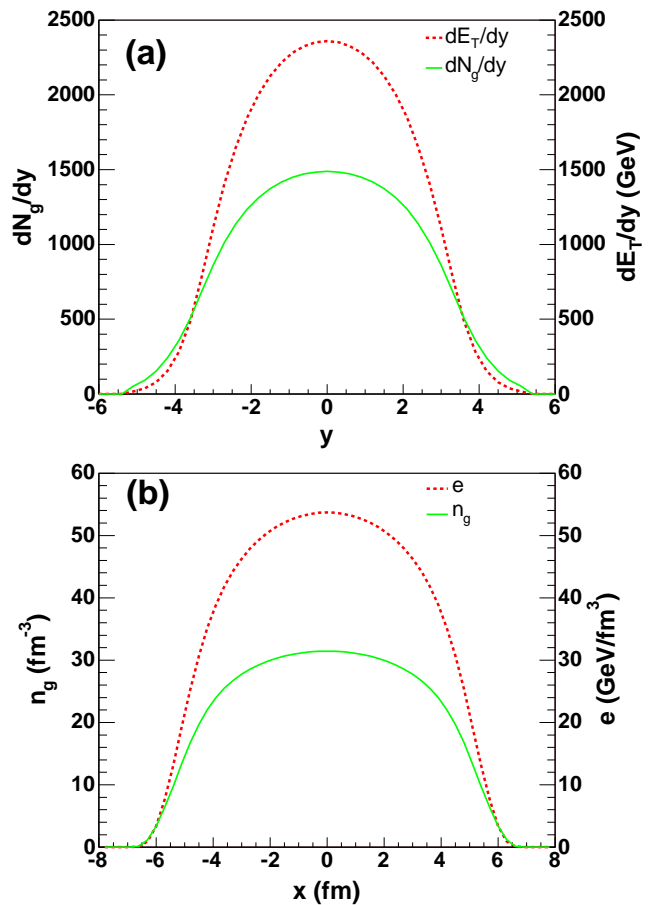


FIG. 1: (a) Rapidity dependence of initial gluon transverse energy (dashed line) and number distribution (solid line) in Au + Au collisions at $\sqrt{s_{NN}} = 200$ GeV at $b = 2.4$ fm. (b) Gluon number and energy densities as functions of a transverse coordinate. Parameters are $\kappa^2 = 3.6$, $K = 0.7$, and $\lambda = 0.2$. As we will discuss in the next subsection, these parameters correspond to an initialization of hydrodynamic simulations which matches the number density of gluons produced by collisions of two CGC's with the parton distribution in hydrodynamic simulations at initial time. The value of κ^2 is chosen so that we reproduce the multiplicity of final hadrons as discussed in Sec. IV. In this procedure, the transverse energy distributions represented by dashed lines are not used as hydrodynamic initial conditions. In the next subsection, we will also discuss the other matching procedure in which the transverse energy distribution is used instead of the gluon number density. In that case, the gluon distributions are factor 1.6 smaller than the results in these figures.

Regardless of the range of the parameter $\lambda = 0.2-0.3$, we find k_T factorization formula gives almost the same shape of rapidity distribution. The initial transverse energy per particle is estimated to be $E_T/N_g \sim 1.6$ GeV at $y = 0$. This is within a range estimated in a numerical simulation of the classical Yang-Mills equation [50, 58].

B. How to connect the CGC to hydrodynamics

In order to obtain a correct initial condition for hydrodynamics, one needs non-equilibrium description for the collisions of heavy nuclei. Especially, whether thermalization is achieved within a few fm/c is a longstanding problem in the physics of heavy ion collisions. The Boltzmann equation with only the elastic parton-parton scattering predicts that the system never reaches a thermal state within a reasonable time scale in heavy ion collisions [40]. Inelastic processes such as $gg \leftrightarrow ggg$ are quite responsible for the equilibration of the system [41, 43]. Although the thermalization process can alter initial conditions, the centrality dependence of total hadron multiplicities is approximately preserved in the CGC initial conditions [42]. QCD plasma instabilities may also play an important role in the thermalization of matter from anisotropic initial conditions and these may help to speed up the equilibration of the plasma [77]. A question of chemical equilibration has been addressed in Refs. [78, 79].

Leaving these problems for the future work, we assume that the system of gluons initially produced from the CGC reaches a kinematically as well as chemically local equilibrate state at a short time scale. We further assume that during being thermalized, the shape of the rapidity distribution is not changed. Thus, we take initial conditions from gluon distribution obtained in the previous subsection based on the CGC.

We consider two simple ways to provide initial conditions from the CGC, i.e., matching of number density (IC- n) and matching of energy density (IC- e). We will compare charged particle distributions from these initial conditions with each other in Sec. IV A. Assuming Bjorken's ansatz $y = \eta_s$ [61] where η_s is the space-time rapidity $\eta_s = (1/2) \ln(x^+/x^-)$, we obtain the number density and the energy density for gluons at a space-time point $(\tau_0, \mathbf{x}_\perp, \eta_s) \equiv (\tau_0, \vec{x})$ from Eq. (1)

$$n_g(\tau_0, \vec{x}) = \frac{dN_g}{\tau_0 d\eta_s d^2x_\perp}, \quad (8)$$

$$e_g(\tau_0, \vec{x}) = \frac{dE_T}{\tau_0 d\eta_s d^2x_\perp}. \quad (9)$$

We take two steps to specify initial conditions in hydrodynamic simulations by using Eqs. (8) or (9). Firstly, we assume that these partons are thermally equilibrated. Secondly, the gluon number density simply represents the $N_f = 3$ parton number density, i.e., the QGP. Although the initial time τ_0 could depend on incident energies (or even on the space coordinate through the saturation scale), we assume a common τ_0 for $\sqrt{s_{NN}} = 130$ and 200 GeV. We note that final particle multiplicity is not sensitive to the initial time τ_0 within a range $0.5 \leq \tau_0 \leq 1.0$ fm/c compared to the energy dependence of the number of initial gluons.

Let us recall the relations among thermodynamical variables, i.e., energy density e , temperature T , and num-

ber density n for the massless free parton system:

$$n = \left(\frac{3}{4}d_q + d_g \right) \frac{\zeta(3)}{\pi^2} T^3, \quad (10)$$

$$e = \left(\frac{7}{8}d_q + d_g \right) \frac{\pi^2}{30} T^4 + B, \quad (11)$$

where $d_q = 2N_c N_s N_f = 36$, $d_g = 2(N_c^2 - 1) = 16$, $\zeta(3) = 1.20206$, and $B (= 486 \text{ MeV/fm}^3)$ is a bag constant which is fixed by matching pressure between the QGP phase and the hadron phase. Thus, we obtain the initial condition in the three-dimensional (3D) space from the number density (IC- n):

$$T(\tau_0, \vec{x}) = \left\{ \frac{\pi^2 n(\tau_0, \vec{x})}{43\zeta(3)} \right\}^{1/3}, \quad (12)$$

or, from the energy density (IC- e)

$$T(\tau_0, \vec{x}) = \left\{ \frac{30[e(\tau_0, \vec{x}) - B]}{47.5\pi^2} \right\}^{1/4}. \quad (13)$$

When the temperature at (τ_0, \vec{x}) is below the critical temperature $T_c = 170$ MeV, the all thermodynamic variables in the site are set to zero. Figure 2 (a) shows the initial parton and energy distributions at the initial time $\tau_0 = 0.6$ fm/c as a function of space-time rapidity η_s . Here $dN/d\eta_s = \tau_0 \int d^2x_\perp n(\tau_0, \vec{x})$ and $dE_T/d\eta_s = \tau_0 \int d^2x_\perp e(\tau_0, \vec{x})$. It should be noted that the assumption of the thermalization for gluons produced from the CGC is to reduce the transverse energy per particle from $E_T/N_g = 1.6$ GeV to $E_T/N_g \sim 1$ GeV within our present parameters. This change should be obtained by non-equilibrium descriptions of pre-thermalization stages. We also plot an initial condition which was employed previously in Ref. [80]. Here we integrate the energy density over all fluid elements with $T > 100$ MeV. The previous initial condition also reproduces the rapidity distribution of final charged hadrons. For longitudinal profiles, it consisted of two regions, i.e., boost invariant region near midrapidity $|\eta'_s| < 2$ and Gaussian shape in forward/backward rapidity regions. Here η'_s is a local space-time rapidity [80] which is shifted from the global midrapidity according to the difference of the thickness of colliding nuclei at x_\perp . The CGC initial condition has no boost invariant region due to the x dependence of unintegrated gluon distribution functions. It is interesting to see the transverse profile from the CGC and to compare with other parametrizations since transverse pressure gradient causes radial flow in hydrodynamics. Three initial conditions in the transverse direction are compared in Fig. 2 (b). In Ref. [80], transverse profile for the initial energy density scales with the number density of the binary collisions (b. c. scaling). On the other hand, the flat profile with smearing near the edge of a nucleus is employed in Ref. [81]. Note that, in Ref. [81], the initial condition is designed for $b = 0$ fm collisions and that cylindrical symmetry is explicitly assumed. For initial energy density

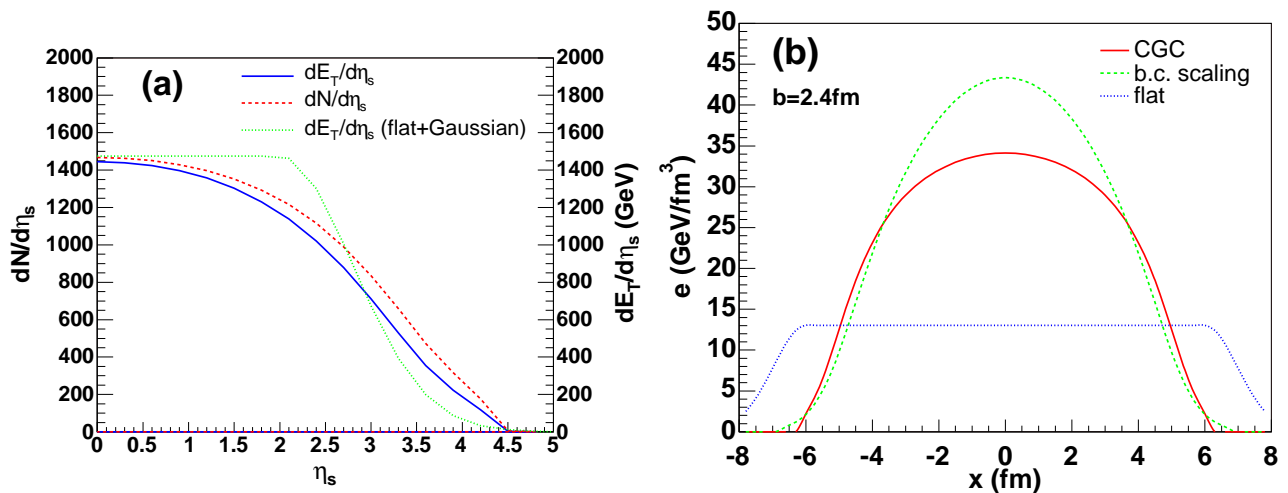


FIG. 2: (a) Space-time rapidity dependence of the initial conditions $dN/d\eta_s$ and $dE_T/d\eta_s$ in Au + Au collisions at $\sqrt{s_{NN}} = 200$ GeV. We also compare the initial energy density distribution with the one which we employed previously in Ref. [80]. (b) Comparison of the transverse profile from IC- n with those in Refs. [80] and [81].

taken from Ref. [81], we take account of correction factors 1.1 and $(1.0/0.6)^{4/3}$ coming from the differences of collision energy and initial time respectively. The value of maximum energy density varies from 13 to 43 GeV/fm³. However, these initial conditions work at least for pion p_T spectrum by adjusting thermal freezeout temperature.

III. HYDRODYNAMICS AND PARTON ENERGY LOSS

In this section, we summarize essential features of the hydro+jet model [17, 63, 64, 65].

Once an initial condition in a hydrodynamic simulation is assigned at an initial time τ_0 , one describes the space-time evolution of thermodynamic variables by numerically solving hydrodynamic equations $\partial_\mu T^{\mu\nu} = 0$ with the help of the EoS, $P = P(e)$. We are assuming baryon free fluids here, so pressure P is a function of energy density e only. In the ideal hydrodynamics, the energy momentum tensor is $T^{\mu\nu} = (e + P)u^\mu u^\nu - P g^{\mu\nu}$, where u^μ is the four fluid velocity. Assuming massless free parton system as discussed in the previous section, the EoS for the QGP phase is $P = (e - 4B)/3$. For the hadron phase, we employ the partial chemical equilibrium model [80] which describes the early chemical freezeout picture by introducing chemical potential for each hadron. Both the phase transition temperature and the chemical freezeout temperature are taken as $T_c = T^{\text{ch}} = 170$ MeV. As a usual prescription, the bag constant $B = 486$ MeV/fm³ is chosen by matching condition for pressure $P_{\text{QGP}}(T_c) = P_{\text{hadron}}(T_c)$. It should be emphasized that, at collider energies, relativistic coordinate in the time and longitudinal directions (τ, η_s) is a substantial choice to describe the evolution in the whole space-time as discussed in Ref. [10, 80]. Within hy-

drodynamic approaches, the studies of centrality and rapidity dependences of observables simultaneously at the collider energies are only accomplished by fully 3D hydrodynamic simulations with the relativistic coordinate. The statistical model and blast wave model analyses tell us that the kinetic (thermal) freezeout temperature T^{th} is smaller than the chemical freezeout temperature T^{ch} [82]. Whereas, both thermal and chemical equilibrium is assumed in the conventional EoS. This means that both freezeouts happen simultaneously and that, consequently, one cannot reproduce the p_T spectra and the particle ratio at the same time. By taking account of the chemical potential accompanied with the number conservation of each stable hadron between chemical freezeout and kinetic freezeout, we obtain the EoS denoting the picture of early chemical freezeout. Note that this EoS results in the almost T^{th} independent p_T slope for pions [80].

For the hard part of the model, we generate momentum spectra of hard partons by PYTHIA 6.2 [83] in which $2 \rightarrow 2$ pQCD hard processes are included. Initial and final state radiations are taken into account for the enhancement of higher-order contributions associated with multiple small-angle parton emission. EKS98 nuclear shadowing [84] is used assuming the impact parameter dependence as in Ref. [85]. We employ the model in Ref. [86] to take into account the multiple initial state scatterings, in which initial k_T is broadened proportional to the number of scatterings. Initial transverse positions of jets at an impact parameter b are determined randomly according to the probability specified by the number of binary collision distribution. Jets are freely propagated up to the initial time τ_0 of hydrodynamic simulations neglecting the possible interactions in the pre-thermalization stages. Jets are assumed to travel with a straight line trajectory in a time step.

Jets lose their energies through gluon emission induced by the dense medium. A lot of work has already done by many authors [23, 24, 25, 26, 27, 28]. Here we employ the Gyulassy-Levai-Vitev (GLV) formula [26] based on an opacity expansion approach which is a relevant formalism for heavy ion collisions. In the original formula, the amount of energy loss is expanded into opacity. Here we take the first order term and neglect the kinematics of emitted gluons

$$\Delta E = C \int_{\tau_0}^{\infty} d\tau \rho(\tau, \mathbf{x}(\tau)) (\tau - \tau_0) \ln \left(\frac{2p_0 \cdot u}{\mu^2 L} \right), \quad (14)$$

where C includes the strong running coupling and color Casimir factors and ρ is a parton density which is to be taken from full 3D hydrodynamic simulations in our approach. $\mu(=0.5\text{GeV})$ is a screening mass and $L(=3\text{fm})$ is a typical length of a medium which can be identified with a lifetime of partonic phase. \mathbf{x} and p_0 are a position and an initial four momentum of a jet. The existence of $\tau - \tau_0$ comes from the so-called LPM effect [87]. In the static medium case, $p_0 \cdot u$ is replaced by an initial energy of a jet E_0 .

In the actual simulations, the coefficient C in Eq. (14) is regarded as an adjustable parameter roughly corresponding to an averaged value over quarks and gluons up to some factor. Our strategy here is that a constant C is set by fitting the PHENIX data on R_{AA} for neutral pions in the most central events at midrapidity [12] and that we next look at the centrality and rapidity dependences. The main reasons are the following. First, we neglect fluctuations of the radiated gluon number [88] in our calculations. An absolute value of the energy loss is about factor two smaller when one takes into account the fluctuations of the radiated gluon number at RHIC [89]. However, the p_T dependence of R_{AA} is found to be the same at RHIC energies [89]. Second, in our present hydrodynamic calculations, it is assumed that massless free gas for quarks ($N_f = 3$) and gluons. However, it is commonly believed that gluons are dominant components in the early stages of collisions at collider energies because of the gluon dominance of the parton structure function at small- x . Thus inclusion of specie dependent factors in C may lead to discrepancy between our hydro+jet results and data.

IV. RESULTS

In this section, we first study the centrality dependence of longitudinal and transverse distribution. Next, the results for the centrality dependence of the nuclear modification factors and back-to-back correlations are presented. Finally, we study the nuclear modification factor at forward rapidity.

Let us summarize our model parameters before showing the results. In the following, we use the parameters $K = 0.7$ and $\lambda = 0.2$ in the gluon distribution of

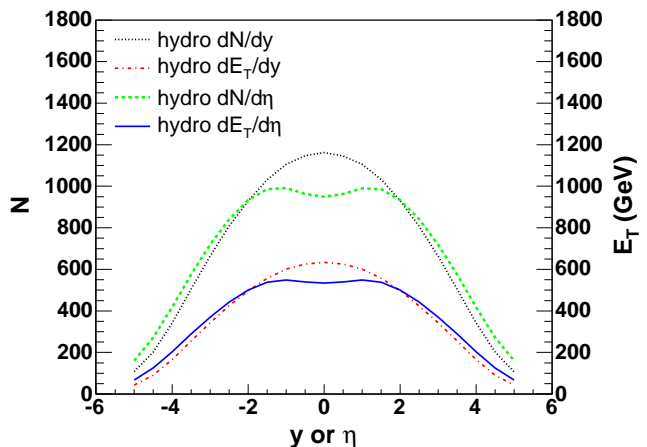


FIG. 3: Rapidity and pseudorapidity distributions of all hadrons in Au + Au collisions at $\sqrt{s_{NN}} = 200$ GeV at $b = 2.4$ fm are compared to the corresponding transverse energy distributions obtained from hydrodynamic simulations with CGC initial condition.

a nucleon. κ depends on how to match initial distributions. For IC- e (IC- n), $\kappa^2 = 2.25(3.6)$. In the hydrodynamic calculation, the kinetic freezeout temperature of $T^{\text{th}} = 100$ MeV and the initial time of $\tau_0 = 0.6$ fm/c are taken. We will not analyze the detailed T^{th} dependence, but will make a short comment on that. A parameter $C = 0.35$ in the parton energy loss formula is fixed by fitting the nuclear modification factor for neutral pions from PHENIX data at 10% centrality [12].

A. Rapidity, centrality, and energy dependences of hadrons

(Pseudo)rapidity distributions of all hadrons and transverse energy in central Au+Au collisions from the hydrodynamic simulation are shown in Fig. 3. Here IC- n is used. As one can compare Fig. 3 with Fig. 2 (a), the effect of the hydrodynamic afterburner is to reduce the transverse energy per particle due to pdV work. We find that $(dE_T/dy)/(dN/dy)|_{y=0} = 0.54$ GeV and $(dE_T/d\eta)/(dN/d\eta)|_{\eta=0} = 0.56$ GeV. Recall that our CGC initial condition from Eq. (1) yields $E_T/N_g = 1.6$ GeV and that it becomes $E_T/N_g = 1.0$ GeV after assuming a thermal state from Fig. 2 (a). The consequence of the hydrodynamic evolution on the shape of rapidity distribution is to make it wider very slightly. Final shape of the rapidity distribution looks like Gaussian which is consistent with recent data from BRAHMS [90]. Our result supports that the KLN calculation [51] which is based on the assumption of parton-hadron duality is a good approximation for the discussion of the shape of pseudorapidity distribution. The number of initial gluons at midrapidity is ~ 1480 (see Fig. 2 (b)), which can be comparable with the number of final hadrons at midrapidity (~ 1160). One see in Fig. 3 that pseudorapidity distribu-

tions for both number and transverse energy are almost flat at mid-rapidity in the range of $|\eta| < 2$, although rapidity distribution has no flat region.

The main difference between the previous [10, 80] and the present initial conditions is whether boost invariant region exists or not (see Fig. 2 (a)). One may ask why the previous initial conditions with boost invariant region near midrapidity can also result in the Gaussian shape in rapidity distributions. It would be instructive here to discuss about the boost invariance for thermodynamic quantities and particle distributions within a hydrodynamic framework. Non-boost invariant dN/dy recently observed by BRAHMS [90] reminds us the so-called Landau picture [91]. Boost invariance for dN/dy is equivalent to the boost invariance of thermodynamic quantities in the original Bjorken assumption [61] in which the length in the η_s direction is assumed to be infinite. However, this is not always true if boost-invariant region for thermodynamic variables is finite. In such a case, rapidity distribution can have *no* boost-invariant region. Let us consider a simple example. Rapidity distribution can be related to the phase-space distribution function via Cooper-Frye formula [92]:

$$\frac{dN}{dy} \propto \int d^2p_T \int f(x, p) p^\mu d\sigma_\mu. \quad (15)$$

Consider, e.g., a finite Bjorken cylinder $|\eta_s| < \eta_0$ with a radius R for massless pions. Assuming no transverse flow, we have $\int d\sigma^\mu = \int d\eta_s \pi R^2 \tau (\cosh \eta_s, \mathbf{0}_\perp, \sinh \eta_s)$ in the case of flat temperature profile. Thus the rapidity distribution becomes

$$\begin{aligned} \frac{dN}{dy} &\propto \int_{-\eta_0}^{\eta_0} d\eta_s \int_0^\infty dp_T p_T^2 \cosh(\eta_s - y) f(\vec{p}) \\ &\propto \int_{-\eta_0}^{\eta_0} d\eta_s \frac{T^3}{\cosh^2(\eta_s - y)}, \end{aligned} \quad (16)$$

where $f(\vec{p}) = 1/(\exp[p_T \cosh(\eta_s - y)/T] - 1)$. This shows rapidity distribution for massless pions in a fluid element at η_s becomes $\propto 1/\cosh^2(y - \eta_s)$. After the above distribution is folded in the finite boost-invariant region $|\eta_s| < \eta_0$, one obtain

$$\frac{dN}{dy} \propto T^3 [\tanh(y + \eta_0) - \tanh(y - \eta_0)]. \quad (17)$$

The resultant rapidity distribution still looks like a Gaussian shape when $\eta_0 < 2$. The flat region starts to appear when $\eta_0 \gtrsim 4$. For more detailed discussions including finite mass effects, see Ref. [93]. We actually reproduced the PHOBOS ($\sqrt{s_{NN}} = 130$ GeV) and the BRAHMS ($\sqrt{s_{NN}} = 200$ GeV) data by using such a Bjorken like initial condition in Ref [10, 65, 80] (for an initial condition, see also Fig. 2 (a)).

In Fig. 4, pseudorapidity distributions of charged hadrons in Au + Au collisions at both $\sqrt{s_{NN}} = 130$ and 200 GeV are compared with the PHOBOS data [94]. Figures 4 (a) and (b) (Figures 4 (c) and (d)) show the results of the initial condition which matches the number

(energy) density distributions for partons between the CGC and hydrodynamics. Impact parameters in each panel are, from top to bottom, 2.4, 4.5, 6.3, 7.9, and 9.1 fm (2.5, 4.4, 6.4, 7.9, and 9.1 fm) for $\sqrt{s_{NN}} = 200$ (130) GeV. These impact parameters are evaluated from the average number of participants at each centrality estimated by PHOBOS [94]. We are not interested in fit for all rapidity region, because we do not include baryon chemical potentials and both the CGC and hydrodynamics break down when density becomes small. The results within the range $|\eta| \lesssim 3-4$ are satisfactory for reproduction of data. Therefore, KLN k_T factorization approach in the CGC provides very good initial conditions for the hydrodynamic simulations which reproduce rapidity, centrality and energy dependences. It should be also emphasized that it is not easy to parametrize such initial conditions which reproduce the data with the same quality as the CGC initial conditions presented here.

In the calculations, we use $\lambda = 0.2$ to get the best fit. However, we find that the results with the range of $\lambda = 0.2-0.3$ are still within experimental error bars. Note that a good description of HERA data has been obtained by parametrization of the saturation scale $Q_s^2 \sim x^\lambda$ with $\lambda \simeq 0.25-0.3$ [38, 39].

Kinetic freeze-out temperature T^{th} which is conventionally fixed by the slope of the transverse momentum spectra is a free parameter in hydrodynamics. However, p_T slope for pions becomes insensitive to T^{th} when one considers early chemical freezeout [80, 95]. But, we need to check the T^{th} dependence on the multiplicity. When we change the kinetic freeze-out temperature, we can also reproduce the data by $\kappa^2 = 3.5, 3.6, 3.7,$ and 3.88 for $T^{\text{th}} = 80, 100, 120,$ and 140 MeV, respectively, for IC- n . We also investigate the τ_0 dependence on the particle multiplicity. We find that the particle yield with $\tau_0 = 1.0$ fm/c is only 4% larger than the case $\tau_0 = 0.6$ fm/c regardless of the centralities as well as energies. This difference can be understood by the $p dV$ work effect.

Mean transverse momenta $\langle p_T \rangle$ for pions, kaons and protons as a function of N_{part} are compared with the PHENIX data [96] in Fig. 5. Since the mean transverse momenta reflects the low p_T physics especially radial flow, contribution from hydrodynamic components at midrapidity is considered in this calculations. Although our results are slightly smaller than the data in central and semicentral regions, the overall trend is consistent with the data. For pions, the semihard spectrum starts to be comparable with the soft spectrum around $p_T = 1.5-2$ GeV/c in this approach. As we will see in the next subsection, we reproduce the p_T spectra for pions by including contribution from jets. So the deviation for pions can be filled by the semihard spectrum. While semihard components for kaons and protons are very small in low and intermediate p_T regions. A little more radial flow is needed to gain the mean transverse momentum in central collisions. More detail discussion will be given in the next subsection.

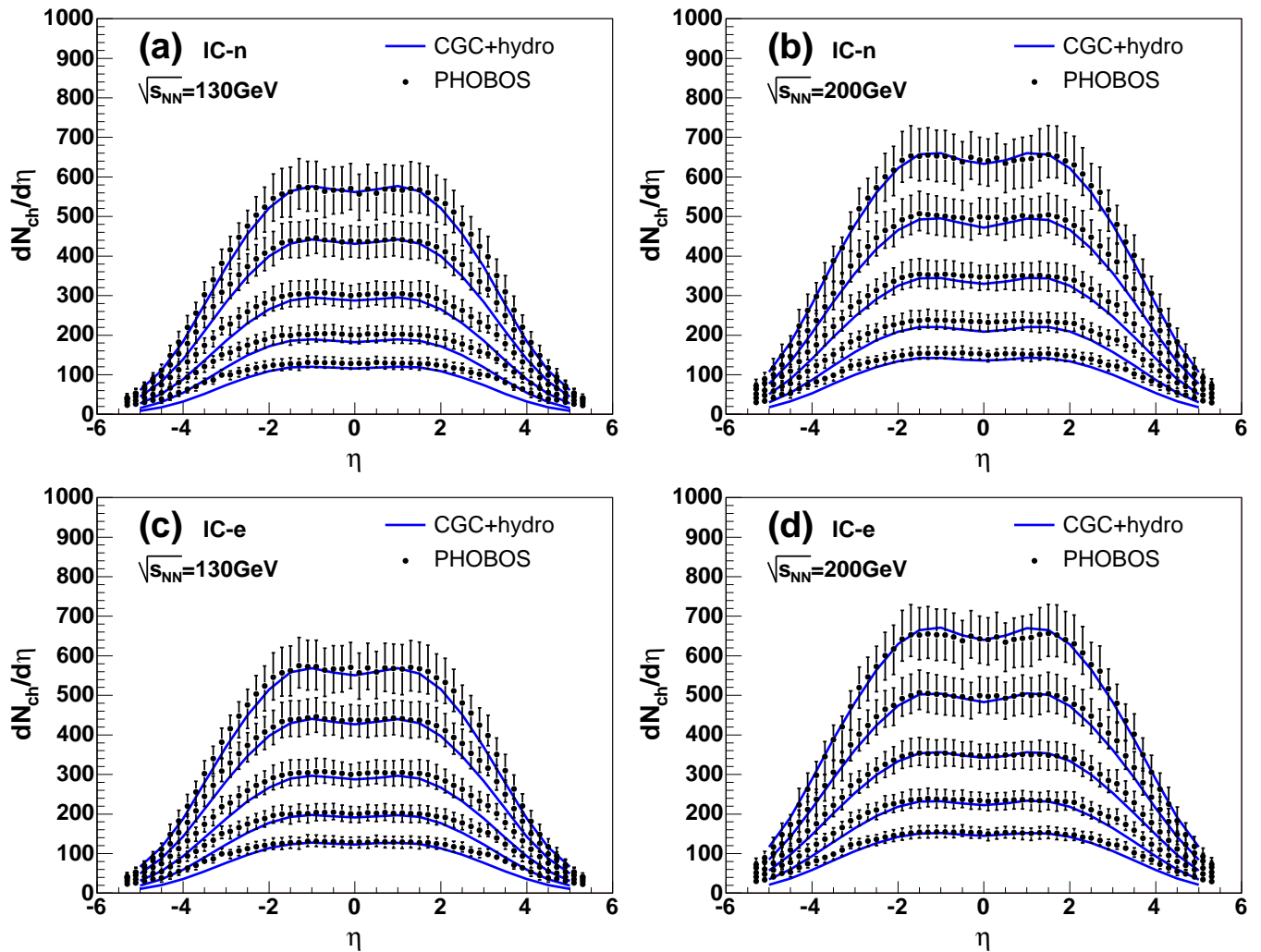


FIG. 4: Pseudorapidity distributions of charged hadrons in Au + Au collisions at $\sqrt{s_{NN}} = 130$ and 200 GeV are compared to the PHOBOS data [94]. For the choice of initial conditions and impact parameters, see text.

B. Jet quenching

In this subsection, we compute the centrality and rapidity dependences of high p_T spectra and nuclear modification factors in the forward rapidity region. All results are obtained by using the initial condition IC- n . In our model, high p_T jets suffer interaction with the local parton density whose evolution is governed by hydrodynamics with the CGC initial conditions. We only take into account parton energy loss in the deconfined matter $T \geq T_c$.

Figure 6 shows that the p_T spectra for identified hadrons from the CGC+hydrojet model are compared with the PHENIX data [96] for several centrality bins. The final p_T spectrum in our approach is the sum of the contribution from fluid elements and from fragmentation of jets. First of all, we see that spectra obtained with the CGC initial condition yield the similar results with the initial condition employed previously [65]. Agreement for

the pion spectra with the PHENIX data is perfect. As mentioned before, hydrodynamic component is insensitive to the choice of T^{th} for the pion spectrum in the chemically frozen hydrodynamics. Slopes of kaons and protons in the model prediction are steeper than that of the data. This indicates that more radial flow is needed for kaons and protons to reduce yields in the low p_T region and to enhance in the intermediate p_T region simultaneously, even after inclusion of the jet components into hydrodynamics. We have checked that freeze-out temperature of $T^{\text{th}} = 80$ MeV still underestimates the slope. RHIC data suggest that initial transverse flow at the time of thermalization τ_0 seems to be important as studied by Kolb and Rapp [95]. This observation is natural because one expects that many rescatterings lead to thermalization. Initial flow profile can be calculated from the classical Yang-Mills fields. Therefore, implementation of Yang-Mills results into the initial condition in the hydrodynamic simulations could considerably im-

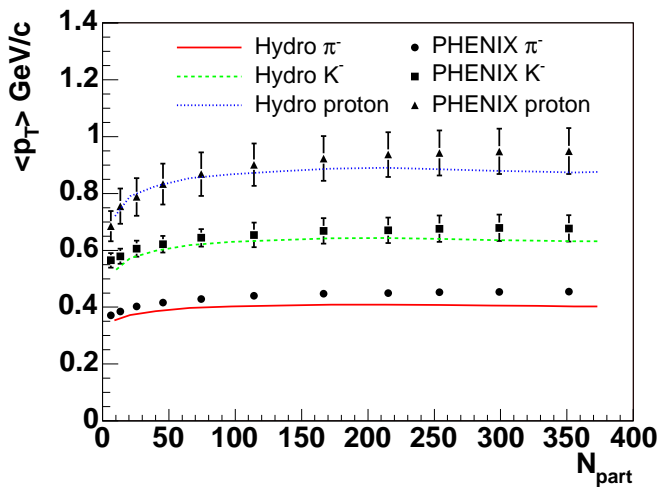


FIG. 5: Mean transverse momenta for pions, kaons and protons as a function of N_{part} . Here contribution only from hydrodynamic components is taken into account. $T^{\text{th}} = 100$ MeV is used for all centralities. Data are taken from Ref. [96]

prove (modify) the hydro results on the transverse momentum distributions. Discrepancy in the high p_T for the proton spectrum might be improved by considering the recombination among hard partons and soft partons [97].

In Fig. 7, we investigate the centrality dependence of the nuclear modification factor for $|\eta| < 0.35$

$$R_{AA}(p_T > 4.5\text{GeV}/c) = \frac{\int_{4.5\text{GeV}/c} dN^{AA}}{N_{\text{coll}} \int_{4.5\text{GeV}/c} dN^{pp}} \quad (18)$$

together with the PHENIX data [98]. Our results only account for the data up to mid-central events and fail to reproduce the data in peripheral collisions. Although this is reasonable because neither CGC nor hydrodynamic description can be reliable in small particle densities, let us study more detailed mechanism.

In the recent studies [18, 19, 99], it is claimed that the centrality dependence of single and dihadron suppression spectra even in peripheral collisions is described by jet quenching in the partonic phase. They assume in their calculation that the parton density is scaled with the number of participants and that the system expands according to (1+1)-dimensional Bjorken expansion [61]. Line integral for the loss of parton energy is evaluated at all densities. This means that there exists only the partonic phase even in very small partonic density and that the effects of phase transition or the hadronic phase are neglected in those calculations. In order to study discrepancy between their results and our results in peripheral collisions, we also estimate the centrality dependence of R_{AA} assuming (1+1)-dimensional Bjorken expansion with the same initial conditions as the 3D ones. In this calculation, the transverse shape of the initial condition is unchanged and the magnitude of the parton density decreases as $\rho(\tau, \mathbf{x}_\perp) = (\tau_0/\tau)\rho(\tau_0, \mathbf{x}_\perp)$. Note that

our transverse profile scales as $\rho \approx Q_s^2(b)/\alpha_s(Q_s^2(b)) \approx \rho_{\text{part}}/\alpha_s(Q_s^2(b))$ at mid-rapidity. pQCD calculations with (1+1)-D Bjorken expansion are performed until the maximum partonic temperature reaches $T = 100$ MeV. When jet quenching happens in $T \geq T_c$, the result of this (1+1)-D Bjorken calculation yields almost the same results as our full 3-D calculations as plotted in the dotted line in Fig. 7. However, when we do not impose a restriction on temperature in the parton energy loss as $T \geq T_c$, the result becomes closer to the data (see solid line in Fig. 7). The difference between these two calculations suggests that there exists a contribution to energy loss besides the purely partonic phase. This can be understood as follows. The density of the system essentially decreases like $\sim 1/\tau$ even in our 3D hydrodynamics. In the case of most central collisions, initial density is so high and most energy loss is likely to occur in the early stages of the collisions. On the other hand, initial energy loss alone is not enough to lose energy of each parton due to small life time of the partonic phase in peripheral collisions. Hence energy loss should last longer until the density of the system becomes small. From above considerations, hadronic interactions [100] seem to be required as well in order to understand the suppression in peripheral collisions, when the bulk matter scales as the $dN/dy \sim N_{\text{part}}/\alpha_s(Q_s^2)$ which is consistent with the centrality dependence of the experimental data contrast to the number of participants scaling.

In Fig. 8, we plot the ratio of the strength of correlation in Au+Au and in pp collisions

$$I_{AA} = \frac{\int_{\Delta\phi_1}^{\Delta\phi_2} d(\Delta\phi) C_2^{AuAu}(\Delta\phi)}{\int_{\Delta\phi_1}^{\Delta\phi_2} d(\Delta\phi) C_2^{pp}(\Delta\phi)} \quad (19)$$

as a function of the number of participants N_{part} together with the experimental data from STAR [16]. $C_2(\Delta\phi)$ is the azimuthal pair distribution per trigger particle,

$$C_2(\Delta\phi) = \frac{1}{N_{\text{trigger}}} \int_{-1.4}^{1.4} d\Delta\eta \frac{dN}{d\Delta\phi d\Delta\eta}. \quad (20)$$

Here $\Delta\phi$ and $\Delta\eta$ are, respectively, the relative azimuthal angle and pseudorapidity between a trigger particle and an associated particle. Charged hadrons in $4 < p_{T,\text{trigger}} < 6$ GeV/c and in $2 < p_{T,\text{associate}} < p_{T,\text{trigger}}$ GeV/c are defined to be trigger particles and associated particles respectively. In the calculation of $C_2(\Delta\phi)$, background is subtracted as in Ref. [17]. Near side correlation is defined as $|\Delta\phi| < 0.75$ radian and away side as $|\Delta\phi| > 2.24$ radian. Our results for the near side correlation show $I_{AA} \sim 1$ for all centralities, because interactions of jets after their hadronization are not included. However the data show $I_{AA} < 1$ for the near side in peripheral collisions. The results on the away side correlation for $N_{\text{part}} \lesssim 100$ deviate from the data, which is consistent with the behavior of R_{AA} as discussed in Fig. 7.

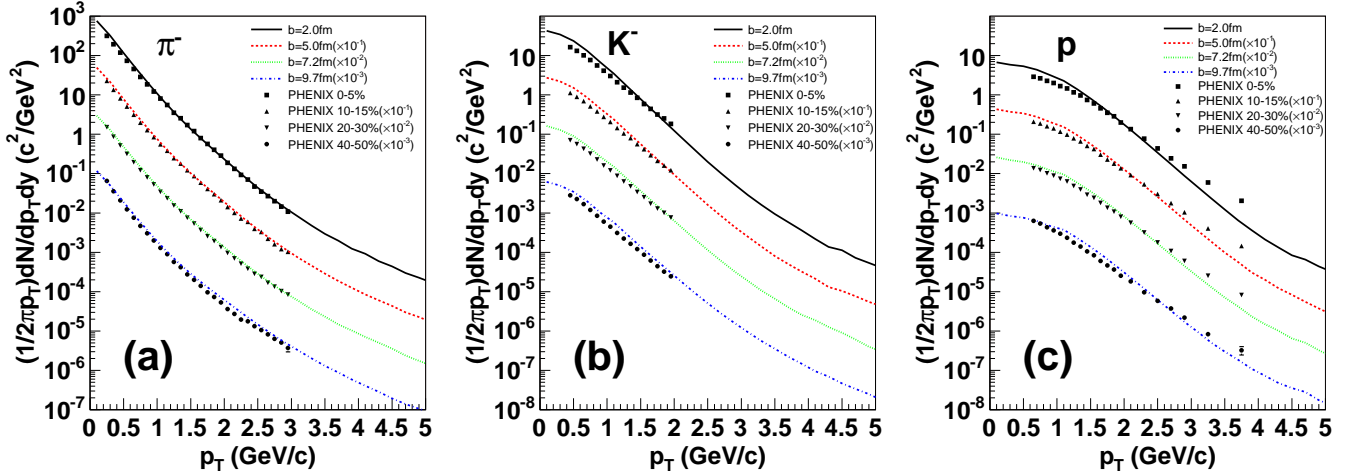


FIG. 6: Centrality dependences of the p_T spectra for (a) pions, (b) kaons, and (c) protons obtained from the CGC+hydrojet model are compared with the PHENIX data [96]. Kinetic freeze-out temperature $T^{\text{th}} = 100$ MeV is used in the calculations,

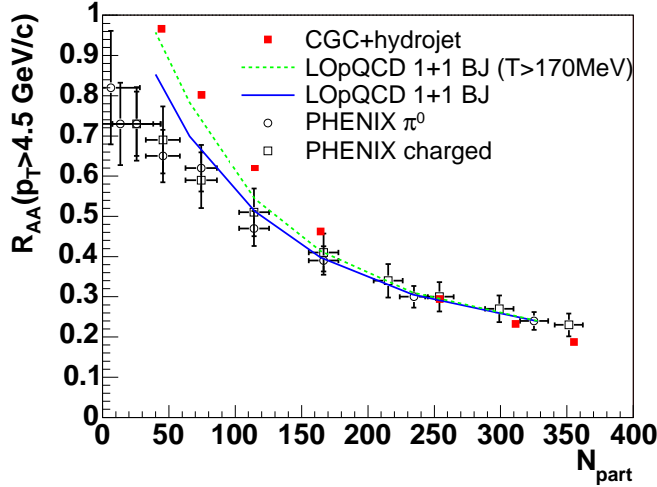


FIG. 7: The CGC+hydrojet result on nuclear modification factor $R_{AA}(p_T > 4.5 \text{ GeV}/c)$ in Au + Au collisions at $\sqrt{s_{NN}} = 200$ is compared with the PHENIX data [98].

C. Nuclear modification factors in the forward rapidity

Recently, the pseudorapidity dependence of nuclear modification factors in both Au+Au and d +Au collisions observed by BRAHMS [15, 56] attracts many theoretical interests in the context of the saturation physics, since one can go deeply into the small x region at forward/backward rapidity. Previously, we investigated the nuclear modification factor in Au+Au collisions

$$R_\eta = \frac{R_{AA}(\eta = 2.2)}{R_{AA}(\eta = 0)} \quad (21)$$

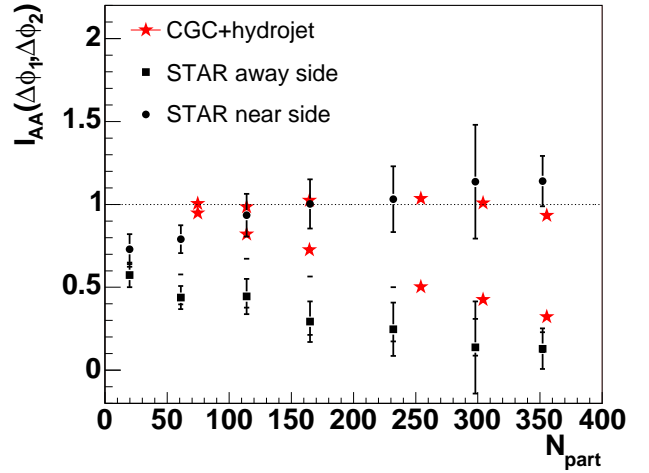


FIG. 8: The CGC+hydrojet result on I_{AA} in Au + Au collisions at $\sqrt{s_{NN}} = 200$ is compared with the STAR data [16].

within the hydro+jet model [64]. In Ref. [64], rapidity dependence of initial parton density was assumed to be flat in $|\eta'_s| < 2$ and R_η was less than unity just because of the difference of p_T slope of semihard spectra between midrapidity and forward/backward rapidity. However, the initial parton density from the CGC has no flat region. Therefore, we should revisit the rapidity dependence of the nuclear modification factor, because partons travel almost straight line and parton energy loss may directly probe the medium at each rapidity bin.

The CGC+hydrojet result for charged hadrons is compared with the BRAHMS data [15] in Fig. 9. We obtain $R_\eta \sim 1$ in the soft region $p_T < 2 \text{ GeV}/c$ which is dominated by the hydrodynamic component. This is the same result as previous work even though initial rapid-

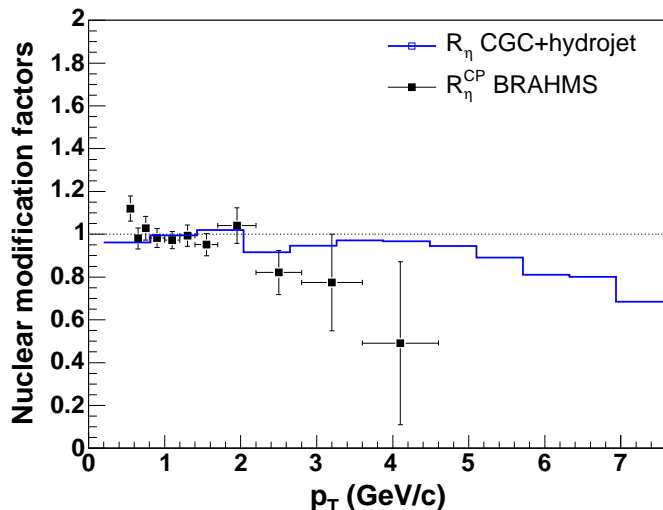


FIG. 9: CGC + hydrojet result for R_η is compared with the BRAHMS data [15] on $R_\eta^{\text{CP}} = R^{\text{CP}}(\eta = 2.2)/R^{\text{CP}}(\eta = 0)$. Note that minijets are produced via pQCD hard $2 \rightarrow 2$ processes, not $2 \rightarrow 1$.

ity distribution is different. The reason is the following. Both initial conditions lead to reproduce the PHOBOS/BRAHMS data on $dN_{\text{ch}}/d\eta$ in which multiplicity at $\eta \sim 2$ is almost the same as at $\eta = 0$. p_T distributions at $\eta = 0$ and 2.2 are similar to each other below $p_T \sim 3$ GeV/c in pp collisions [64]. We also find that the effect of radial flow at $\eta_s \sim 2$ is also the same as at midrapidity. Hence R_{AA} in the low p_T regions are insensitive to pseudorapidity within this range. One may worry about the effect of pseudorapidity dependent Jacobian $J = p/E = \sqrt{1 - m^2/(p_T^2 \cosh^2 \eta + m^2)}$ on p_T distributions. However, this is already canceled in the calculation of R_{AA} before obtaining its ratio R_η in Eq. (21).

Situation is different in the high p_T part. our result starts to deviate from unity at $p_T \sim 5$ GeV/c since p_T slope from pQCD hard collisions becomes much steeper for larger rapidity. On the other hand, experimental data deviates prior to our result. Note that the discrepancy between the present result and our previous result [64] comes from the initial longitudinal shape of the energy density shown in Fig. 2 (a). In the previous parametrization of the initial energy density, dynamical evolution at midrapidity was almost the same as at the *space-time rapidity* $\eta_s = 2$. Thus $R_\eta < 1$ came from purely the difference of p_T slope between midrapidity and forward rapidity. While, in the initial condition from the CGC, initial energy density at midrapidity is slightly larger than at $\eta_s = 2$. Therefore, the “slope” effect is compensated by the dynamical effect. This result indicates that p_T spectrum in forward rapidity region is already suppressed by the initial state effect. If this is the case, instead of using conventional pQCD approach, we may need to include x -evolution for the calculation of p_T spectrum up to $p_T = 10$ GeV/c that corresponds to $x < 0.01$

at $y = 2$ [55, 73]. As demonstrated in Ref. [74], study of the back-to-back correlations at forward rapidity will clarify the influence of parton saturation in the CGC.

V. SUMMARY AND OUTLOOK

We developed a dynamical model for the description of the time evolution of high dense matter created in heavy ion collisions at high energies on the basis of the CGC in colliding nuclei, hydrodynamic evolution for produced bulk matter, and the parton energy loss in the medium. In this approach, collisions of two CGC’s are calculated for the initial condition of hydrodynamic simulations. Thermalized dense partons produced from colliding two CGC’s are evolved hydrodynamically and also used to evaluate energy loss of high- p_T partons.

We have shown that hydrodynamic simulations with the CGC initial conditions describe centrality, rapidity, and energy dependences of charged hadron multiplicity very well. The best agreement for the transverse momentum distribution was obtained for pions with the hydrodynamic component and the quenched hard jet component. However, our results on kaons and protons indicated that we need other mechanisms to understand kaon and proton transverse momentum spectra from low to high- p_T . The centrality dependence of nuclear modification factors and the back-to-back correlation were found to be consistent with the data up to the centrality of $N_{\text{part}} > 100-150$. Finally we compared the nuclear modification factor at $\eta = 2.2$ to BRAHMS data by using this new initial conditions. We found that, when the QGP parton density at the forward rapidity is smaller than at mid-rapidity, suppression of hard jet from pQCD calculation which is supplemented by DGLAP evolution is not enough to account for the data. It suggests that the small- x evolution will be necessary for the calculation of particle spectra at forward rapidities at RHIC.

Our main objective has been developing a consistent dynamical framework for the time evolution of both soft matter and hard jets. In order to meet this goal, many remains are to be done in the near future. Each component should be improved to obtain a better description of the whole of the stages of heavy ion collisions.

For initial conditions, more sophisticated unintegrated gluon distribution should be used as mentioned in Sec. II. Numerical solutions of the classical Yang-Mills equations in (2+1) dimension [49] can be used for transverse profile in the boost invariant hydrodynamics. Quantum evolution is important for the LHC energy and forward/backward rapidity regions at RHIC. (3+1)-D Yang-Mills solutions in which renormalization group evolution of the color charges is implemented are strongly demanded.

The ideal massless QGP EoS is employed in the deconfined phase in our present hydrodynamic model. The EoS in hydrodynamics should be consistent with lattice QCD results. For example, one can parametrize recent lattice

results by a resonance gas model for hadronic phase [101]. In connection with jet quenching phenomena, it is argued that the small non-perturbative screening mass which is observed in lattice simulations [102] leads to reduction of the amount of jet quenching in the vicinity of phase transition region [103]. Therefore, one expect that jet quenching would strongly depend on the EoS [104].

One of the important goals in the jet tomography is to constrain the evolving gluon density. Therefore, removing the free parameter C in Eq. (14) will be one of the most important future work within our approach in order to see that gluon density provided by the hydrodynamic simulation is truly consistent with the energy loss of partons. In order to achieve this goal, we need to extend our hydrodynamics and use more complicated formula for the parton energy loss at the same time. For the more realistic description of chemical compositions of quarks and gluons in the deconfinement phase, we can solve hydrody-

amic equations together with rate equations for number densities of quarks and gluons [79]. This also affects jet quenching through the different cross section among gg , gq , and qq processes. The kinematic effect of radiated gluons, fluctuations, or higher order terms in the opacity expansion in GLV formula should be taken into account in the energy loss of hard partons.

Acknowledgments

The authors are grateful to A. Dumitru, U. Heinz, J. Jalilian-Marian, D. Kharzeev, L. McLerran, D. Teaney, and R. Venugopalan for useful comments. The work of T.H. was supported by RIKEN. Research of Y.N. was supported by the DOE under Contract No. DE-FG03-93ER40792.

-
- [1] K. H. Ackermann *et al.*, STAR Collaboration, Phys. Rev. Lett. **86**, 402 (2001).
 - [2] P. Huovinen, in *Quark Gluon Plasma 3*, edited by R.C. Hwa and X.N. Wang (World Scientific, Singapore, 2004); P. F. Kolb and U. Heinz, in *Quark Gluon Plasma 3*, edited by R.C. Hwa and X.N. Wang (World Scientific, Singapore, 2004).
 - [3] T. Hirano, nucl-th/0403042.
 - [4] P.F. Kolb, P. Huovinen, U. Heinz, and H. Heiselberg, Phys. Lett. B **500**, 232 (2001); P. Huovinen, P.F. Kolb, U.W. Heinz, P.V. Ruuskanen, and S.A. Voloshin, *ibid.* B **503**, 58 (2001).
 - [5] C. Alt *et al.*, NA49 Collaboration, Phys. Rev. C **68**, 034903 (2003).
 - [6] G. Agakichiev *et al.*, CERES/NA45 Collaboration, Phys. Rev. Lett. **92**, 032301 (2004).
 - [7] P. F. Kolb, J. Sollfrank, and U. W. Heinz, Phys. Rev. C **62**, 054909 (2000).
 - [8] C. Adler *et al.*, STAR Collaboration, Phys. Rev. C **66**, 034904 (2002).
 - [9] B. B. Back *et al.*, PHOBOS Collaboration, Phys. Rev. Lett. **89**, 222301 (2002).
 - [10] T. Hirano, Phys. Rev. C **65**, 011901 (2002).
 - [11] M. Gyulassy, I. Vitev, X. N. Wang, and B. W. Zhang, in *Quark Gluon Plasma 3*, edited by R.C. Hwa and X.N. Wang (World Scientific, Singapore, 2004); A. Kovner and U. A. Wiedemann, in *Quark Gluon Plasma 3*, edited by R.C. Hwa and X.N. Wang (World Scientific, Singapore, 2004).
 - [12] K. Adcox *et al.*, PHENIX Collaboration, Phys. Rev. Lett. **88**, 022301 (2002); S. S. Adler *et al.*, Phys. Rev. Lett. **91**, 072301 (2003).
 - [13] C. Adler *et al.*, STAR Collaboration, Phys. Rev. Lett. **89**, 202301 (2002); K. Adcox *et al.*, Phys. Lett. B **561**, 82 (2003).
 - [14] B. B. Back *et al.*, PHOBOS Collaboration, Phys. Lett. B **578**, 297 (2004).
 - [15] I. Arsene *et al.*, BRAHMS Collaboration, Phys. Rev. Lett. **91**, 072305 (2003).
 - [16] C. Adler *et al.*, STAR Collaboration, Phys. Rev. Lett. **90**, 082302 (2003).
 - [17] T. Hirano and Y. Nara, Phys. Rev. Lett. **91**, 082301 (2003).
 - [18] X. N. Wang, nucl-th/0305010.
 - [19] X. N. Wang, Phys. Lett. B **579**, 299 (2004).
 - [20] B. B. Back *et al.*, PHOBOS Collaboration, Phys. Rev. Lett. **91**, 072302 (2003).
 - [21] S. S. Adler *et al.*, PHENIX Collaboration, Phys. Rev. Lett. **91**, 072303 (2003).
 - [22] J. Adams *et al.*, STAR Collaboration, Phys. Rev. Lett. **91**, 072304 (2003).
 - [23] R. Baier, Y.L. Dokshitzer, S. Peigné, and D. Schiff, Phys. Lett. B **345**, 277 (1995); R. Baier, Y. L. Dokshitzer, A. H. Mueller, S. Peigne, and D. Schiff, Nucl. Phys. **B483**, 291 (1997); R. Baier, Y. L. Dokshitzer, A. H. Mueller, S. Peigné, and D. Schiff, Nucl. Phys. **B484**, 265 (1997); R. Baier, Y. L. Dokshitzer, A. H. Mueller, and D. Schiff, Nucl. Phys. B **531**, 403 (1998); R. Baier, D. Schiff, and B.G. Zakharov, Ann. Rev. Nucl. Part. Sci. **50**, 37 (2000).
 - [24] B. G. Zakharov, JETP Lett. **63**, 952 (1996).
 - [25] U.A. Wiedemann, Nucl. Phys. **B588**, 303 (2000); Nucl. Phys. **A690**, 731 (2001); C. A. Salgado and U. A. Wiedemann, Phys. Rev. Lett. **89**, 092303 (2002).
 - [26] M. Gyulassy, P. Lévai, and I. Vitev, Nucl. Phys. **B594**, 371 (2001); **B571**, 197 (2000); Phys. Rev. Lett. **85**, 5535 (2000).
 - [27] X. f. Guo and X. N. Wang, Phys. Rev. Lett. **85**, 3591 (2000); X. N. Wang and X. f. Guo, Nucl. Phys. A **696**, 788 (2001); E. Wang and X. N. Wang, Phys. Rev. Lett. **87**, 142301 (2001). Phys. Rev. Lett. **89**, 162301 (2002).
 - [28] P. Arnold, G. D. Moore and L. G. Yaffe, JHEP **0111**, 057 (2001); JHEP **0206**, 030 (2002); JHEP **0301**, 030 (2003).
 - [29] I. Vitev and M. Gyulassy, Phys. Rev. Lett. **89**, 252301 (2002).
 - [30] C. A. Salgado and U. A. Wiedemann, Phys. Rev. D **68**, 014008 (2003).
 - [31] A. H. Mueller, Nucl. Phys. B **572**, 227 (2000).
 - [32] L. V. Gribov, E. M. Levin, and M. G. Ryskin, Phys.

- Rept. **100**, 1 (1983).
- [33] E. Iancu and R. Venugopalan, in *Quark Gluon Plasma 3*, edited by R.C. Hwa and X.N. Wang (World Scientific, Singapore, 2004).
- [34] L. D. McLerran and R. Venugopalan, Phys. Rev. D **49**, 2233 (1994); **49**, 3352 (1994); **50**, 2225 (1994).
- [35] J. Jalilian-Marian, A. Kovner, L. McLerran, and H. Weigert, Phys. Rev. D **55**, 5414 (1997); J. Jalilian-Marian, A. Kovner, A. Leonidov, and H. Weigert, Nucl. Phys. B **504**, 415 (1997), Phys. Rev. D **59**, 014014 (1999), Phys. Rev. D **59**, 034007 (1999), [Erratum-ibid. D **59**, 099903 (1999)]; J. Jalilian-Marian, A. Kovner, and H. Weigert, Phys. Rev. D **59**, 014015 (1999).
- [36] A. Kovner, J. G. Milhano, and H. Weigert, Phys. Rev. D **62**, 114005 (2000); A. Kovner and J. G. Milhano, Phys. Rev. D **61**, 014012 (2000); H. Weigert, Nucl. Phys. A **703**, 823 (2002).
- [37] E. Iancu, A. Leonidov, and L. D. McLerran, Nucl. Phys. A **692**, 583 (2001); E. Ferreira, E. Iancu, A. Leonidov, and L. McLerran, Nucl. Phys. A **703**, 489 (2002).
- [38] K. Golec-Biernat and M. Wusthoff, Phys. Rev. D **59**, 014017 (1999); D **60**, 114023 (1999).
- [39] E. Iancu, K. Itakura, and S. Munier, hep-ph/0310338.
- [40] A. H. Mueller, Phys. Lett. **B475**, 220 (2000); A. Dumitru and M. Gyulassy, Phys. Lett. **B494**, 215 (2000); J. Bjorker and R. Venugopalan, Phys. Rev. C **63**, 024609 (2001); J. Serreau and D. Schiff, JHEP **0111**, 039 (2001).
- [41] R. Baier, A. H. Mueller, D. Schiff, and D. T. Son, Phys. Lett. B **502**, 51 (2001).
- [42] R. Baier, A. H. Mueller, D. Schiff, and D. T. Son, Phys. Lett. B **539**, 46 (2002).
- [43] G. R. Shin and B. Muller, J. Phys. G **28**, 2643 (2002).
- [44] A. Kovner, L. McLerran, and H. Weigert, Phys. Rev. D **52**, 3809 (1995); D **52**, 6231 (1995); M. Gyulassy and L. McLerran, Phys. Rev. C **56**, 2219 (1997).
- [45] Y. V. Kovchegov and D. H. Rischke, Phys. Rev. C **56**, 1084 (1997); S. G. Matinyan, B. Müller and D. H. Rischke, *ibid.* C **56**, 2191 (1997); C**57**, 1927 (1998); Xiao-feng Guo, *ibid.* D **59**, 094017 (1999).
- [46] Y. V. Kovchegov and A. H. Mueller, Nucl. Phys. B **529**, 451 (1998).
- [47] A. Dumitru and L. D. McLerran, Nucl. Phys. A **700**, 492 (2002); A. Dumitru and J. Jalilian-Marian, Phys. Rev. Lett. **89**, 022301 (2002); Phys. Lett. B **547**, 15 (2002).
- [48] A. Krasnitz and R. Venugopalan, Nucl. Phys. **B557**, 237 (1999); Phys. Rev. Lett. **86**, 1717 (2001); **84**, 4309 (2000).
- [49] A. Krasnitz, Y. Nara, and R. Venugopalan, Phys. Rev. Lett. **87**, 192302 (2001); Nucl. Phys. **A717**, 268 (2003).
- [50] T. Lappi, Phys. Rev. C **67**, 054903 (2003).
- [51] D. Kharzeev and M. Nardi, Phys. Lett. B **507**, 121 (2001); D. Kharzeev and E. Levin, *ibid.* B **523**, 79 (2001); D. Kharzeev, E. Levin, and M. Nardi, arXiv:hep-ph/0111315; D. Kharzeev, E. Levin and M. Nardi, Nucl. Phys. A **730**, 448 (2004).
- [52] Y. V. Kovchegov and K. L. Tuchin, Nucl. Phys. A **708**, 413 (2002); Nucl. Phys. A **717**, 249 (2003).
- [53] K. Itakura, Y. V. Kovchegov, L. McLerran, and D. Teaney, Nucl. Phys. A **730**, 160 (2004).
- [54] J. L. Albacete, N. Armesto, A. Kovner, C. A. Salgado and U. A. Wiedemann, Phys. Rev. Lett. **92**, 082001 (2004); D. Kharzeev, Y. V. Kovchegov, and K. Tuchin, Phys. Rev. D **68**, 094013 (2003); J. Jalilian-Marian, Y. Nara, and R. Venugopalan, Phys. Lett. B **577**, 54 (2003). J. P. Blaizot, F. Gelis, and R. Venugopalan, hep-ph/0402256; hep-ph/0402257; E. Iancu, K. Itakura, and D. N. Triantafyllopoulos, hep-ph/0403103; R. Baier, A. H. Mueller, and D. Schiff, hep-ph/0403201.
- [55] J. Jalilian-Marian, nucl-th/0402080.
- [56] R. Debbé, nucl-ex/0403052.
- [57] P. Huovinen, P. V. Ruuskanen, and J. Sollfrank, Nucl. Phys. A **650**, 227 (1999).
- [58] A. Krasnitz, Y. Nara, and R. Venugopalan, Nucl. Phys. A **727**, 427 (2003).
- [59] A. Krasnitz, Y. Nara, and R. Venugopalan, Phys. Lett. B **554**, 21 (2003).
- [60] A. Bazilevsky *et al.*, PHENIX Collaboration, Nucl. Phys. A **715**, 486c (2003).
- [61] J. D. Bjorken, Phys. Rev. D **27**, 140 (1983).
- [62] M. Gyulassy, I. Vitev, X. N. Wang, and P. Huovinen, Phys. Lett. B **526**, 301 (2002).
- [63] T. Hirano and Y. Nara, Phys. Rev. C **66**, 041901(R) (2002); Nucl. Phys. **A721**, 277 (2003).
- [64] T. Hirano and Y. Nara, Phys. Rev. C **68**, 064902 (2003).
- [65] T. Hirano and Y. Nara, Phys. Rev. C **69**, 034908 (2004).
- [66] Y. V. Kovchegov, Nucl. Phys. A **692**, 557 (2001).
- [67] L. V. Gribov, E. M. Levin, and M. G. Ryskin, Phys. Lett. B **100**, 173 (1981).
- [68] E. Laenen and E. Levin, Ann. Rev. Nucl. Part. Sci. **44**, 199 (1994).
- [69] A. Szczurek, Acta Phys. Polon. B **34**, 3191 (2003).
- [70] I. Balitsky, Nucl. Phys. B **463**, 99 (1996).
- [71] Y. V. Kovchegov, Phys. Rev. D **60**, 034008 (1999).
- [72] E. Iancu, K. Itakura, and L. McLerran, Nucl. Phys. A **708**, 327 (2002).
- [73] D. Kharzeev, E. Levin, and L. McLerran, Phys. Lett. B **561**, 93 (2003).
- [74] D. Kharzeev, E. Levin, and L. McLerran, hep-ph/0403271.
- [75] E. Iancu, K. Itakura, and L. McLerran, Nucl. Phys. A **724**, 181 (2003).
- [76] R. Baier, A. Kovner, and U. A. Wiedemann, Phys. Rev. D **68**, 054009 (2003).
- [77] J. Randrup and S. Mrowczynski, Phys. Rev. C **68**, 034909 (2003); P. Arnold, J. Lenaghan, and G. D. Moore, JHEP **0308**, 002 (2003); P. Romatschke and M. Strickland, Phys. Rev. D **68**, 036004 (2003); Phys. Rev. D **69**, 065005 (2004); S. Mrowczynski, A. Rebhan and M. Strickland, arXiv:hep-ph/0403256.
- [78] E. V. Shuryak, Phys. Rev. Lett. **68**, 3270 (1992).
- [79] T. S. Biro, E. van Doorn, B. Muller, M. H. Thoma, and X. N. Wang, Phys. Rev. C **48**, 1275 (1993); P. Levai, B. Muller, and X. N. Wang, Phys. Rev. C **51**, 3326 (1995); D. K. Srivastava, M. G. Mustafa, and B. Muller, Phys. Rev. C **56**, 1064 (1997); D. M. Elliott and D. H. Rischke, Nucl. Phys. A **671**, 583 (2000).
- [80] T. Hirano and K. Tsuda, Phys. Rev. C **66**, 054905 (2002).
- [81] K. Morita, S. Muroya, C. Nonaka and T. Hirano, Phys. Rev. C **66**, 054904 (2002).
- [82] See, for example, E. V. Shuryak, Nucl. Phys. **A661**, 119 (1999); U. Heinz, *ibid.* **A661**, 140 (1999).
- [83] T. Sjostrand, P. Eden, C. Friberg, L. Lonnblad, G. Miu, S. Mrenna, and E. Norrbin, Comput. Phys. Commun. **135**, 238 (2001).

- [84] K. J. Eskola, V. J. Kolhinen, and P. V. Ruuskanen, Nucl. Phys. **B535**, 351 (1998); K. J. Eskola, V. J. Kolhinen, and C. A. Salgado, Eur. Phys. J. C. **9**, 61 (1999).
- [85] V. Emel'yanov, A. Khodinov, S. R. Klein, and R. Vogt, Phys. Rev. C **61**, 044904 (2000).
- [86] X. N. Wang, Phys. Rev. C **61**, 064910 (2000); Phys. Lett. B **565**, 116 (2003).
- [87] L. D. Landau and I. P. Pomeranchuk, Dokl. Akad. Nauk SSSR, Ser. A **92**, 535 (1953); **92** 735 (1953); A. B. Migdal, Phys. Rev. **103**, 1811 (1956).
- [88] R. Baier, Y. L. Dokshitzer, A. H. Mueller, and D. Schiff, JHEP **0109**, 033 (2001).
- [89] M. Gyulassy, P. Levai, and I. Vitev, Phys. Lett. B **538**, 282 (2002).
- [90] I. G. Bearden *et al.*, BRAHMS Collaboration, nucl-ex/0403050.
- [91] L. D. Landau, Izv. Akad. Nauk SSSR Ser. Fiz. **17**, 51 (1953).
- [92] F. Cooper and G. Frye, Phys. Rev. D **10**, 186 (1974).
- [93] E. Schnedermann, J. Sollfrank, and U. W. Heinz, Phys. Rev. C **48**, 2462 (1993).
- [94] B. B. Back *et al.*, Phys. Rev. Lett. **91**, 052303 (2003).
- [95] P. F. Kolb and R. Rapp, Phys. Rev. C **67**, 044903 (2003).
- [96] S. S. Adler *et al.*, PHENIX Collaboration, nucl-ex/0307022.
- [97] R. C. Hwa and C. B. Yang, nucl-th/0401001.
- [98] S. S. Adler *et al.*, PHENIX Collaboration, nucl-ex/0308006.
- [99] A. Drees, H. Feng, and J. Jia, arXiv:nucl-th/0310044.
- [100] K. Gallmeister, C. Greiner, and Z. Xu, Phys. Rev. C **67**, 044905 (2003); W. Cassing, K. Gallmeister, and C. Greiner, Nucl. Phys. A **735**, 277 (2004).
- [101] F. Karsch, K. Redlich, and A. Tawfik, Phys. Lett. B **571**, 67 (2003).
- [102] O. Kaczmarek, F. Karsch, E. Laermann, and M. Lutgemeier, Phys. Rev. D **62**, 034021 (2000).
- [103] A. Dumitru and R. D. Pisarski, Phys. Lett. B **525**, 95 (2002).
- [104] A. Dumitru, private communication.